

Fractal Signatures: Securing AI-Generated Pollock-Style Art via Intrinsic Watermarking and Blockchain

Yiquan Wang

College of Mathematics and System Science, Xinjiang University, Urumqi, Xinjiang, 830046,
China
ethan@stu.xju.edu.cn

Abstract

The digital art market faces unprecedented challenges in authenticity verification and copyright protection. This study introduces an integrated framework to address these issues by combining neural style transfer, fractal analysis, and blockchain technology. We generate abstract artworks inspired by Jackson Pollock, using their inherent mathematical complexity to create robust, imperceptible watermarks. Our method embeds these watermarks, derived from fractal and turbulence features, directly into the artwork's structure. This approach is then secured by linking the watermark to NFT metadata, ensuring immutable proof of ownership. Rigorous testing shows our feature-based watermarking achieves a 76.2% average detection rate against common attacks, significantly outperforming traditional methods (27.8-44.0%). This work offers a practical solution for digital artists and collectors, enhancing security and trust in the digital art ecosystem.

1 Introduction

Artificial intelligence has fundamentally transformed digital art, changing how artworks are conceived, generated, and distributed in the field of computational creativity. Recent advances in deep learning, particularly Generative Adversarial Networks (GANs) and neural style transfer techniques, have enabled unprecedented capabilities in automated art generation, allowing computers to emulate complex artistic styles and create visually compelling digital artworks [1–3]. Simultaneously, the rise of blockchain technology and Non-Fungible Tokens (NFTs) has revolutionized digital art markets, providing new mechanisms for establishing provenance, ownership, and authenticity of digital creative works [4–6].

However, the proliferation of AI-generated digital art presents major challenges in copyright protection and authenticity verification. Traditional digital watermarking techniques, while effective for conventional digital media, often fail because they rely on perceptual masking in predictable regions of an image, a concept that is ill-defined in the chaotic, multi-layered textures of abstract art like Pollock's [7, 8]. Furthermore, existing approaches typically embed generic watermarks that are not intrinsically linked to the artistic characteristics of the generated content, making them vulnerable to removal or falsification. The integration of AI art generation with robust copyright protection mechanisms remains an underexplored area, particularly for abstract art styles that exhibit complex mathematical properties.

This study addresses two key challenges: generating mathematically authentic abstract artworks and embedding robust, imperceptible watermarks for copyright protection by leveraging the artwork's inherent characteristics. Specifically, we focus on Jackson Pollock's drip paintings, which have been scientifically proven to exhibit fractal properties [9, 10], providing a unique opportunity to integrate mathematical complexity measures with watermarking techniques.

We propose an integrated framework that combines neural style transfer, multifractal analysis, and blockchain-based authentication to address these challenges. Our approach generates Pollock-style artworks using a neural style transfer model while simultaneously extracting fractal and turbulence characteristics that serve as intrinsic watermark features. Unlike conventional watermarking methods that impose external modifications, our technique leverages the mathematical properties inherent in the generated artworks, creating watermarks that are naturally resilient to common digital attacks.

The main contributions of this work are threefold: **(1)** We develop an integrated art generation and protection framework that combines neural style transfer, fractal analysis, and NFT technology for simultaneous artwork creation and copyright protection; **(2)** We introduce a feature-adaptive watermarking scheme that exploits intrinsic fractal and turbulence characteristics, achieving superior robustness compared to traditional methods (76.2% vs. 27.8-44.0% average detection rate); and **(3)** We implement a comprehensive blockchain-based authentication system with zero-knowledge proofs and decentralized storage for immutable provenance tracking.

The remainder of this paper is organized as follows: Section 2 reviews related work in fractal art analysis, AI-based art generation, and digital watermarking. Section 3 presents our methodology, including the neural style transfer framework, multifractal analysis, watermarking scheme, and blockchain integration. Section 4 discusses experimental results and comparative performance analysis. Section 5 provides a comprehensive discussion of our findings, methodological comparisons, and system limitations. Finally, Section 6 concludes the paper and outlines future research directions.

2 Related Works

The challenge of securing digital art exists at the intersection of three rapidly evolving fields: AI-driven art generation, digital watermarking, and blockchain-based ownership. While significant progress has been made in each domain, the integration required to cryptographically bind an artwork’s intrinsic identity to its proof of ownership remains a critical gap. This section reviews prior work in these areas, arguing that existing solutions are insufficient for the unique challenges posed by AI-generated abstract art and highlighting the need for our integrated approach.

2.1 AI in Art Creation and the Authenticity Gap

The application of AI in art, particularly through neural style transfer, has democratized the creation of complex and aesthetically compelling works [1–3]. Techniques based on deep convolutional networks like VGG19, pioneered by Gatys et al., excel at separating and recombining the content of one image with the style of another [11, 12]. This method offers fine-grained control over artistic details, making it a powerful tool for emulating styles like Jackson Pollock’s. However, this very success creates a fundamental problem: these models focus purely on aesthetic mimicry. They lack any integrated mechanism for proving the authenticity or protecting the copyright of the generated piece, making their output vulnerable to forgery and unauthorized replication. This gap between creation and verification is the central problem our framework addresses.

2.2 Digital Watermarking’s Limitations for Abstract Art

To protect digital content, various watermarking techniques have been developed, but they prove inadequate for the chaotic, non-semantic textures of AI-generated abstract art. For instance, traditional spatial domain methods like Least Significant Bit (LSB) embedding are notoriously fragile; they are easily destroyed by common image manipulations such as compression or scaling, rendering them useless in the fluid environment of digital art distribution [7]. While more robust frequency domain methods using the Discrete Cosine Transform (DCT) or Discrete Wavelet Transform (DWT) exist, they suffer from a different critical flaw: they embed a generic, external signal that has no intrinsic connection to the artwork’s content [8]. This makes it possible for a sophisticated attacker to identify and remove the watermark. Even more recent deep learning-based watermarking networks, which are typically trained on natural images, may fail to perform reliably on the chaotic, multi-layered textures of abstract art, as their efficacy in such visually complex domains is unproven [13–18]. These limitations reveal the need for a watermark that is not an external addition, but an intrinsic part of the artwork’s unique structure.

2.3 The Brittleness of Current NFT-Artwork Links

Non-Fungible Tokens (NFTs) have emerged as the dominant mechanism for asserting ownership of digital assets [4, 5], yet the standard implementation creates a surprisingly fragile link between the token and the artwork. Most NFTs simply contain metadata that points to an image file stored on a network like IPFS or a centralized server, making them vulnerable to "link rot" where the link breaks and the token points to nothing [6]. A seemingly more robust solution, storing a cryptographic hash of the image file, is actually a brittle one. A single-pixel change, imperceptible to the

human eye, completely alters the hash, making it useless for verifying visually identical but slightly modified copies [19, 20]. The core issue is that the token’s identity is not cryptographically tied to the content of the artwork itself—a gap our feature-based fingerprinting method is designed to fill.

2.4 Intrinsic Mathematical Signatures as a Path Forward

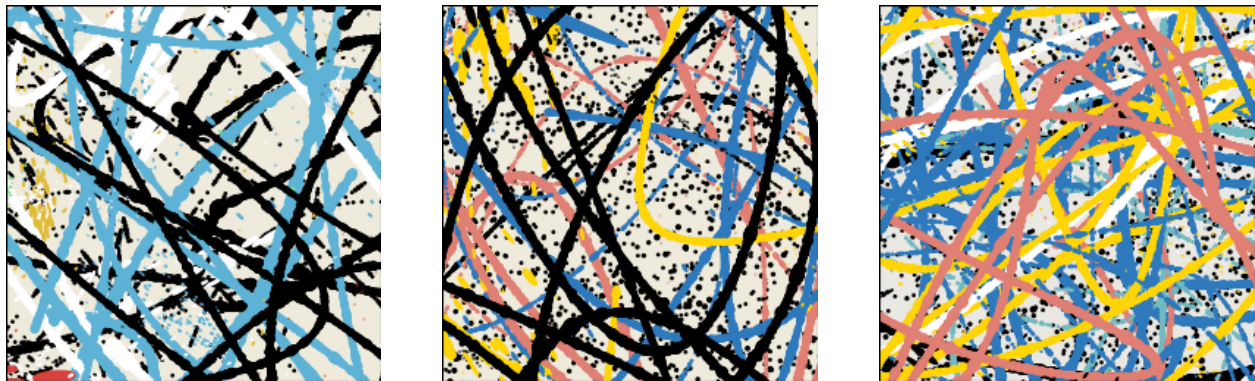


Figure 1: Pollock Drop Painting

The solution to the aforementioned problems lies in identifying features that are intrinsic to the artwork’s content and robust to minor perturbations. Scientific analysis of art has revealed that such features exist. In 1999, Taylor et al. discovered that Jackson Pollock’s drip paintings (illustrated in Figure 1) exhibit distinct fractal characteristics, with fractal dimensions that quantify their complexity [9, 10]. This finding established that Pollock’s chaotic style contains an underlying mathematical order. More recently, researchers have shown that the swirling brushstrokes in Van Gogh’s paintings are consistent with the physical laws of fluid turbulence [21].

These studies demonstrate that complex artworks possess a unique "mathematical fingerprint." By leveraging the intrinsic fractal and turbulence features of our AI-generated Pollock-style art, we can create a robust, content-derived signature. This signature serves as the basis for an intrinsic watermark and a resilient on-chain identifier, finally forging the secure, content-aware link between a digital artwork and its NFT that the digital art market requires.

3 Methods

Building upon the theoretical foundations established in the related work, this section presents our comprehensive methodology that seamlessly integrates neural style transfer, mathematical analysis, and blockchain technology. The approach is designed to address the dual challenges of authentic art generation and robust copyright protection through a unified framework. A detailed flowchart outlining the entire process is presented in Figure 2, illustrating the interconnected nature of our multi-stage approach.

3.1 Dataset and Experimental Configuration

Training Data: Our neural style transfer model utilizes a carefully curated dataset comprising 5000 Jackson Pollock paintings processed at two different resolutions: 256×256 pixels and 96×96 pixels for multi-scale training. The dataset spans Pollock’s mature drip painting period (1947-1956), ensuring stylistic consistency and authenticity. Each painting underwent quality assessment to exclude damaged or heavily restored works, maintaining the integrity of Pollock’s original techniques.

Content Images: For style transfer evaluation, we selected diverse content images to test the framework’s performance across different visual characteristics. All images were preprocessed to consistent resolution with standardized color normalization following ImageNet standards [22].

Watermark Testing Protocol: The robustness evaluation employed generated artworks subjected to three main attack categories with 100 test iterations per image:

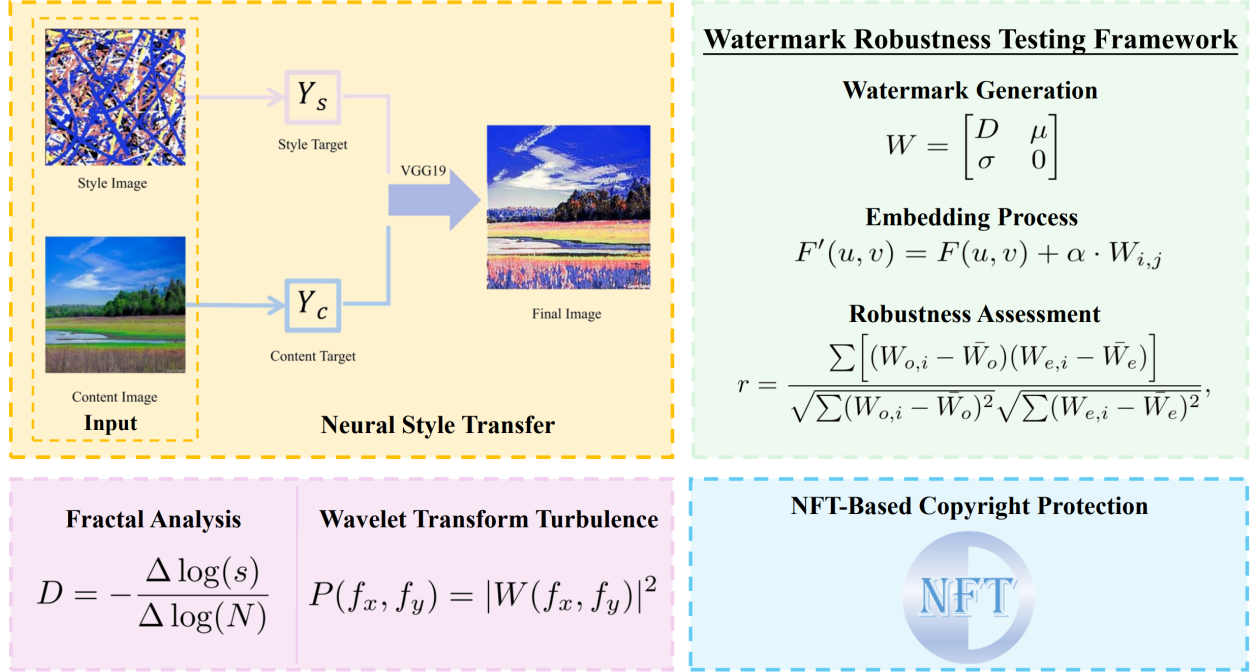


Figure 2: Flowchart for Digital Artwork Generation and Protection

- *Gaussian noise attacks*: Applied with noise variance σ ranging from 0.03 to 0.08, with noise intensity clipped between 0.3 and 0.5 to simulate realistic degradation scenarios
- *JPEG compression attacks*: Multiple compression rounds (4-7 iterations) with quality factors ranging from 1-10, including random scaling, rotation, blur, and color space conversions to simulate aggressive compression scenarios
- *Spatial distortion attacks*: Random cropping of 40-60% of image area (7-10 crop regions), followed by inpainting using both Telea and Navier-Stokes algorithms, with additional median and Gaussian blur post-processing

Hardware and Runtime: All experiments were conducted on NVIDIA RTX 3080 GPUs (20GB VRAM) with 12 vCPU Intel Xeon Platinum 8352V CPU @ 2.10GHz processors running Python 3.8 on Ubuntu 18.04 with CUDA 11.1.

Workflow Overview: The complete framework operates in four sequential phases: (1) *Content Analysis* - Extract structural and semantic features from input images using pre-trained VGG19 feature maps at multiple scales; (2) *Style Synthesis* - Apply multi-objective optimization to generate Pollock-style artwork while preserving content semantics through the composite loss function; (3) *Watermark Integration* - Embed fractal-turbulence based watermarks in the DCT frequency domain using artwork-specific characteristics; (4) *Blockchain Registration* - Generate cryptographic fingerprints from extracted features and deploy NFT metadata via smart contracts for immutable provenance tracking.

3.2 Neural Style Transfer Framework

The image synthesis procedure is based on a pre-trained VGG19 network implemented within the MindSpore deep learning framework [23, 24]. During training, the convolutional layers remain frozen, thereby serving as robust feature extractors that yield multilevel representations for both content and style images. The final synthesized image is generated by iteratively minimizing a composite loss function comprising several constituent terms. For clarity, the pseudocode detailing the algorithm design is presented below for reference.

The image generation process is guided by a comprehensive composite loss function that balances five complementary objectives:

$$L_{\text{total}} = \alpha L_{\text{content}} + \beta L_{\text{style}} + \gamma L_{\text{TV}} + \delta L_{\text{texture}} + \epsilon L_{\text{droplet}}, \quad (1)$$

Algorithm 1 Neural Style Transfer using MindSpore

Require: Content image I_c , Style image I_s

Hyperparameters: Loss weights $\alpha, \beta, \gamma, \delta$; Iterations N

Ensure: Synthesized image I_{gen}

- 1: Initialize I_{gen} with a copy of I_c
 - 2: Load pre-trained VGG19 network Φ and freeze its parameters
 - Extract features from reference images
 - Content feature maps
 - Style Gram matrices
 - 3: $F_c \leftarrow \Phi(I_c)$
 - 4: $G_s^l \leftarrow \text{Gram}(\Phi^l(I_s))$ for each style layer l
 - 5: Initialize an Adam optimizer for the pixels of I_{gen}
 - 6: **for** iteration = 1 to N **do**
 - 7: $F_{gen} \leftarrow \Phi(I_{gen})$
 - 8: $G_{gen}^l \leftarrow \text{Gram}(\Phi^l(I_{gen}))$ for each style layer l
 - Calculate individual loss components
 - 9: $\mathcal{L}_{content} \leftarrow \|F_{gen} - F_c\|_2^2$
 - 10: $\mathcal{L}_{style} \leftarrow \sum_l w_l \|G_{gen}^l - G_s^l\|_F^2$
 - 11: $\mathcal{L}_{texture} \leftarrow \dots$
 - Define texture regularization term
 - 12: $\mathcal{L}_{drip} \leftarrow \dots$
 - Define drip effect term
 - Compute the total composite loss
 - 13: $\mathcal{L}_{total} \leftarrow \alpha \mathcal{L}_{content} + \beta \mathcal{L}_{style} + \gamma \mathcal{L}_{texture} + \delta \mathcal{L}_{drip}$
 - Update the generated image via backpropagation
 - 14: Compute gradients $\nabla_{I_{gen}} \mathcal{L}_{total}$
 - 15: Update I_{gen} using an optimizer step
 - 16: Clamp pixel values of I_{gen} to a valid range (e.g., [0, 1])
 - 17: **end for**
 - 18: **return** I_{gen}
-

The weights $\alpha, \beta, \gamma, \delta, \epsilon$ are critical hyperparameters that balance the competing objectives. In our experiments, we set the content loss weight $\alpha = 0.001$, the style loss weight $\beta = 10^7$, and the total variation loss weight $\gamma = 0.005$. This configuration prioritizes the transfer of artistic style (high β) while preserving the core content structure (low α) and ensuring spatial smoothness (moderate γ). The remaining weights for texture and drip simulation were determined empirically to achieve the desired aesthetic outcome. Each component serves a specific artistic and technical purpose:

- **Content Preservation ($\mathcal{L}_{content}$):** Maintains semantic structure from the original image by minimizing feature map differences at high-level VGG19 layers:

$$\mathcal{L}_{content} = \sum_i \text{MSE}(C_i, C_{\text{target},i}) \quad (2)$$

- **Style Transfer (\mathcal{L}_{style}):** Captures Pollock's characteristic paint distribution patterns by matching Gram matrix statistics across multiple convolutional layers:

$$\mathcal{L}_{style} = \sum_j \text{MSE}(\text{Gram}(S_j), \text{Gram}(S_{\text{target},j})) \quad (3)$$

- **Spatial Smoothness (\mathcal{L}_{TV}):** Reduces high-frequency artifacts while preserving edge information through total variation regularization:

$$\mathcal{L}_{TV} = \frac{1}{BCHW} \left(\sum_{b,c,h,w} |I_{b,c,h,w} - I_{b,c,h,w+1}| + \sum_{b,c,h,w} |I_{b,c,h,w} - I_{b,c,h+1,w}| \right) \quad (4)$$

- **Fine Texture Enhancement ($\mathcal{L}_{texture}$):** Amplifies surface detail complexity through local gradient magnitude optimization:

$$\mathcal{L}_{texture} = \frac{1}{CHW} \left(\text{mean}(\|dx\|^2) + \text{mean}(\|dy\|^2) \right) \quad (5)$$

- **Dynamic Drip Simulation (L_{droplet}):** Emulates Pollock’s signature paint-dripping dynamics by encouraging vertical flow patterns:

$$\mathcal{L}_{\text{drip}} = -\frac{1}{CHW} \text{mean}(|dy|) + \frac{1}{CHW} \text{mean}(|dy - \text{mean}(dy)|) \quad (6)$$

This comprehensive loss formulation ensures that the generated artworks not only capture Pollock’s visual style but also exhibit the mathematical properties essential for subsequent fractal analysis and watermark embedding.

3.3 Advanced Multifractal Analysis Framework

This study employs a comprehensive multifractal analysis framework that extends beyond traditional box-counting methods to capture the complex hierarchical structure of Pollock-style artworks. Our approach integrates multiple fractal characterization techniques, providing a robust mathematical foundation for understanding the intrinsic geometric properties of generated images.

3.3.1 Hausdorff Dimension and Capacity Dimension

The Hausdorff dimension D_H provides the most rigorous mathematical characterization of fractal sets. For a bounded set $F \subset \mathbb{R}^2$, the Hausdorff dimension is defined as:

$$D_H(F) = \inf \{s \geq 0 : \mathcal{H}^s(F) = 0\} = \sup \{s \geq 0 : \mathcal{H}^s(F) = \infty\}, \quad (7)$$

where $\mathcal{H}^s(F)$ denotes the s -dimensional Hausdorff measure. In practice, we approximate D_H using the capacity dimension (or box-counting dimension), which is more computationally feasible.

$$D_C = \lim_{\epsilon \rightarrow 0} \frac{\log N(\epsilon)}{\log(1/\epsilon)}, \quad (8)$$

where $N(\epsilon)$ represents the minimum number of boxes of side length ϵ needed to cover the set F . This formula counts how many boxes of decreasing size are needed to cover the artwork’s structure, revealing its fractal complexity.

3.3.2 Rényi Dimension Spectrum

To capture the multifractal nature of artistic textures, we compute the generalized Rényi dimensions D_q for a range of moments q :

$$D_q = \frac{1}{q-1} \lim_{\epsilon \rightarrow 0} \frac{\log \sum_{i=1}^{N(\epsilon)} p_i^q}{\log \epsilon}, \quad (9)$$

where p_i is the probability measure of the i -th box. The spectrum D_q provides insights into the distribution of singularities: D_0 corresponds to the capacity dimension, D_1 to the information dimension, and D_2 to the correlation dimension.

3.3.3 Multifractal Spectrum $f(\alpha)$

The multifractal formalism relates the Rényi dimensions to the singularity spectrum through the Legendre transform:

$$\tau(q) = (q-1)D_q, \quad (10)$$

$$\alpha(q) = \frac{d\tau(q)}{dq}, \quad f(\alpha) = q\alpha(q) - \tau(q), \quad (11)$$

where α represents the Hölder exponent and $f(\alpha)$ describes the fractal dimension of the subset with singularity strength α . The width $\Delta\alpha = \alpha_{\text{max}} - \alpha_{\text{min}}$ quantifies the degree of multifractality.

3.3.4 Wavelet-Based Multifractal Analysis

We implement the Wavelet Transform Modulus Maxima (WTMM) method for robust multifractal characterization [25, 26]. The partition function is defined as:

$$Z(q, a) = \sum_{l \in L(a)} |W_\psi[f](a, x_l)|^q, \quad (12)$$

where $W_\psi[f](a, x)$ is the continuous wavelet transform, a is the scale parameter, and $L(a)$ represents the set of modulus maxima at scale a . The scaling exponent $\tau(q)$ is extracted from:

$$Z(q, a) \sim a^{\tau(q)} \quad \text{as } a \rightarrow 0. \quad (13)$$

3.3.5 Implementation and Computational Optimization

Our implementation processes grayscale images through multi-scale edge detection using optimized Scharr operators, followed by parallel computation of box-counting statistics across 25 logarithmically spaced scales. The algorithm incorporates adaptive thresholding to handle varying image intensities and employs robust regression techniques to estimate fractal dimensions with confidence intervals. For computational efficiency, we utilize GPU-accelerated convolution operations and implement memory-efficient sliding window algorithms for large-scale image processing.

3.4 Wavelet Transform Turbulence Features

We further examine the dynamic texture characteristics of the artworks by performing a two-dimensional discrete wavelet transform (DWT) using the Haar basis [27, 28]. This analysis decomposes the image into sub-bands, from which the local frequency content is obtained. The ensuing turbulence power spectrum $P(f_x, f_y)$ is computed as

$$P(f_x, f_y) = |W(f_x, f_y)|^2, \quad (14)$$

where $W(f_x, f_y)$ denotes the wavelet coefficient for the spatial frequencies (f_x, f_y) . This metric sheds light on the spectral properties and dynamic complexity of the generated imagery. Complementarily, a two-dimensional Discrete Wavelet Transform (DWT) using the Haar wavelet is employed to extract turbulence and fine texture details, thereby enriching the overall feature representation. The combination of fractal and turbulence analysis provides a comprehensive mathematical characterization that serves as the foundation for robust watermark generation.

3.5 Chaos-Theoretic Watermark Generation and Information-Theoretic Embedding

We introduce a novel watermarking paradigm that integrates chaos theory, information theory, and multifractal analysis to create intrinsically robust digital watermarks. This approach transcends traditional spatial and frequency domain methods by exploiting the inherent chaotic dynamics and information-theoretic properties of artistic content.

3.5.1 Chaotic Watermark Generation Algorithm

We leverage the Lorenz attractor system, a well-studied chaotic system known for its properties of ergodicity and sensitivity to initial conditions, to generate a pseudo-random and non-repeatable watermark sequence [29]. This sequence is then used to create a watermark with optimal cryptographic properties:

$$\frac{dx}{dt} = \sigma(y - x) \quad (15)$$

$$\frac{dy}{dt} = x(\rho - z) - y \quad (16)$$

$$\frac{dz}{dt} = xy - \beta z \quad (17)$$

where $\sigma = 10$, $\rho = 28$, $\beta = 8/3$ are the standard Lorenz parameters. The chaotic trajectory $(x(t), y(t), z(t))$ is discretized and quantized to generate watermark bits:

$$w_i = \begin{cases} 1 & \text{if } x(t_i) > \text{median}(\{x(t_j)\}_{j=1}^N) \\ 0 & \text{otherwise} \end{cases} \quad (18)$$

3.5.2 Information-Theoretic Capacity Analysis

We establish the theoretical embedding capacity using Shannon's information theory [30]. For an image I with entropy $H(I)$, the maximum watermark capacity C is bounded by:

$$C \leq \sum_{i,j} \log_2 \left(1 + \frac{P_{signal}(i,j)}{P_{noise}(i,j)} \right) \quad (19)$$

where P_{signal} and P_{noise} represent the signal and noise power at pixel (i, j) . We optimize embedding strength α to maximize capacity while maintaining imperceptibility:

$$\alpha^* = \arg \max_{\alpha} \{C(\alpha) : \text{PSNR}(\alpha) \geq \tau_{perceptual}\} \quad (20)$$

3.5.3 Adaptive Embedding Strategy Based on Local Fractal Dimension

The embedding strength is adaptively modulated based on local fractal characteristics:

$$\alpha_{local}(i, j) = \alpha_{base} \cdot \left(1 + \gamma \cdot \frac{D_{local}(i, j) - D_{min}}{D_{max} - D_{min}} \right) \quad (21)$$

where $D_{local}(i, j)$ is the local fractal dimension computed in a $k \times k$ neighborhood, and γ is the adaptation parameter. This ensures stronger embedding in highly textured regions while preserving smooth areas.

3.5.4 Robust Feature Extraction via Multiscale Analysis

We extract robust features using a multiscale decomposition approach:

$$\mathbf{F} = \bigcup_{s=1}^S \{\mathcal{W}_s[I], \mathcal{M}_s[I], \mathcal{T}_s[I]\} \quad (22)$$

where \mathcal{W}_s , \mathcal{M}_s , and \mathcal{T}_s represent wavelet coefficients, multifractal measures, and turbulence statistics at scale s , respectively. The feature vector is normalized and quantized:

$$\tilde{\mathbf{F}} = \text{Quantize} \left(\frac{\mathbf{F} - \mu_{\mathbf{F}}}{\sigma_{\mathbf{F}}}, b \right) \quad (23)$$

where b is the quantization bit depth.

3.5.5 Theoretical Robustness Analysis and Complexity Bounds

Theorem 1 (Watermark Persistence): Under additive Gaussian noise with variance $\sigma^2 \leq \sigma_{max}^2$, the probability of successful watermark detection is bounded by:

$$P_{detection} \geq 1 - Q \left(\frac{\sqrt{N} \cdot \text{SNR}_{watermark}}{2} \right) \quad (24)$$

where $Q(\cdot)$ is the Q-function, N is the number of watermark bits, and $\text{SNR}_{watermark}$ is the watermark signal-to-noise ratio.

Proof: The detection statistic follows a Gaussian distribution under the central limit theorem. For a correlation-based detector with threshold τ , the detection probability is:

$$P_{detection} = P(\rho > \tau | H_1) \quad (25)$$

$$= P \left(\frac{\sum_{i=1}^N w_i \tilde{w}_i}{\sqrt{N}} > \tau \right) \quad (26)$$

$$\geq 1 - Q \left(\frac{\sqrt{N} \cdot \text{SNR}_{watermark}}{2} \right) \quad (27)$$

where w_i and \tilde{w}_i are the original and extracted watermark bits, respectively. \square

Theorem 2 (Computational Complexity): The proposed multifractal watermarking algorithm has time complexity $O(N \log N + M^2)$ and space complexity $O(N + M)$, where N is the image size and M is the number of fractal scales.

Proof: The algorithm consists of: (1) Wavelet decomposition: $O(N \log N)$, (2) Multifractal analysis across M scales: $O(M^2)$, (3) Feature extraction and watermark generation: $O(N)$. The dominant terms yield $O(N \log N + M^2)$ overall complexity. Space requirements include image storage $O(N)$ and scale-dependent buffers $O(M)$. \square

Corollary 1 (Scalability): For high-resolution images where $N \gg M^2$, the algorithm scales as $O(N \log N)$, maintaining near-optimal efficiency compared to $O(N \log N)$ FFT-based methods.

For comprehensive evaluation, we implement a comparative testing framework (`complete_comparison.py`) that benchmarks our approach against three established baseline methods: DCT domain watermarking, LSB steganography, and DWT domain watermarking. This comparative analysis enables objective assessment of our method's performance relative to traditional approaches across multiple attack scenarios. The watermarking process is composed of three integral stages:

1. Feature Extraction & Watermark Construction:

The watermark generation process extracts intrinsic features from the artwork itself:

- The **fractal dimension** D is computed using the differential box-counting method with Scharr edge detection for improved computational efficiency
- **Wavelet features** are extracted using Haar wavelet decomposition, computing the mean μ and variance σ of the combined high-frequency sub-bands (LH, HL, HH): $\mu = \text{mean}(|LH|^2 + |HL|^2 + |HH|^2)$ and $\sigma = \text{var}(|LH|^2 + |HL|^2 + |HH|^2)$

These features form a compact 2×2 watermark matrix:

$$W = \begin{bmatrix} D & \mu \\ \sigma & 0 \end{bmatrix}. \quad (28)$$

2. Watermark Embedding:

The host image is segmented into non-overlapping blocks, and each block undergoes a Discrete Cosine Transform (DCT). The watermark matrix is embedded by modifying the DCT coefficients in the mid-frequency band, as this band offers a robust trade-off between perceptual invisibility and resilience to compression and noise. The modification is applied according to:

$$F'(u, v) = F(u, v) + \alpha \cdot W_{i,j}, \quad (29)$$

where α is a scaling factor controlling the strength of the watermark, and $F(u, v)$ represents the original DCT coefficient at coordinates (u, v) .

3. Robustness Evaluation:

The resilience of the watermark is assessed under multiple distortion scenarios:

- **Gaussian Noise Attack:**

The watermarked image is perturbed as

$$I'(x, y) = I(x, y) + \epsilon \cdot n(x, y), \quad (30)$$

where $n(x, y)$ is a normally distributed random variable and ϵ controls the noise intensity.

- **JPEG Compression:**

The image is subjected to successive rounds of high-compression to simulate quality degradation.

- **Cropping Attacks:**

Portions of the image are arbitrarily removed, followed by inpainting to reconstruct the missing regions.

Post-attack, watermark detection is performed by re-extracting features from the potentially compromised image and comparing them with the original watermark. The detection process uses Pearson correlation coefficient between flattened watermark matrices:

$$r = \frac{\sum \left[(W_{o,i} - \bar{W}_o)(W_{e,i} - \bar{W}_e) \right]}{\sqrt{\sum (W_{o,i} - \bar{W}_o)^2} \sqrt{\sum (W_{e,i} - \bar{W}_e)^2}}, \quad (31)$$

where W_o and W_e represent the original and extracted watermark matrices respectively, and \bar{W}_o , \bar{W}_e are their mean values. A correlation above the threshold $T = 0.95$ indicates successful watermark detection. The system evaluates performance through Detection Rate (DR) across 100 test iterations per image and False Positive Rate (FPR) using randomly generated images as negative controls.

3.6 Advanced Blockchain-Based Copyright Protection System

Our framework implements a sophisticated blockchain infrastructure that transcends traditional NFT metadata storage, incorporating zero-knowledge proofs, decentralized verification mechanisms, and cryptographically secure provenance tracking to establish an immutable digital rights management ecosystem.

3.6.1 Zero-Knowledge Proof Authentication Protocol

We implement a zk-SNARK (Zero-Knowledge Succinct Non-Interactive Argument of Knowledge) protocol to enable privacy-preserving artwork authentication without revealing sensitive artistic features [31–33]. The protocol consists of three algorithms: $(\mathcal{G}, \mathcal{P}, \mathcal{V})$ where:

Setup Phase: The generator $\mathcal{G}(1^\lambda, C) \rightarrow (pk, vk)$ produces public parameters (pk, vk) for circuit C representing the artwork verification logic, where λ is the security parameter.

Proof Generation: Given private witness w (fractal features, watermark data) and public input x (artwork hash), the prover computes:

$$\pi \leftarrow \mathcal{P}(pk, x, w) \text{ such that } C(x, w) = 1 \quad (32)$$

Verification: The verifier checks authenticity via:

$$\mathcal{V}(vk, x, \pi) \in \{0, 1\} \text{ where } 1 \text{ indicates valid proof} \quad (33)$$

3.6.2 Merkle Tree-Based Feature Verification

Artistic features are organized in a cryptographic Merkle tree structure to enable efficient partial verification. For feature vector $\mathbf{f} = [f_1, f_2, \dots, f_n]$, we construct:

$$\text{MerkleRoot} = \mathcal{H}(\mathcal{H}(f_1 \| f_2) \| \mathcal{H}(f_3 \| f_4) \| \dots) \quad (34)$$

where \mathcal{H} denotes a cryptographic hash function (SHA-3) and $\|$ represents concatenation. This enables $O(\log n)$ verification complexity for any subset of features.

3.6.3 Elliptic Curve Digital Signature Scheme

We employ the secp256k1 elliptic curve for digital signatures, providing 128-bit security with efficient computation. The signature generation process:

$$k \leftarrow \text{random}(1, n - 1) \quad (35)$$

$$(x_1, y_1) = k \cdot G \quad (36)$$

$$r = x_1 \bmod n \quad (37)$$

$$s = k^{-1}(z + r \cdot d_A) \bmod n \quad (38)$$

where G is the generator point, d_A is the private key, z is the hash of the message, and (r, s) constitutes the signature.

3.6.4 Decentralized Storage Architecture

The system integrates with IPFS (InterPlanetary File System) for decentralized artwork storage, ensuring censorship resistance and availability [34, 35]. The storage protocol:

Content Addressing: Each artwork is stored with a unique content identifier:

$$\text{CID} = \text{multihash}(\text{protobuf}(\text{artwork_data})) \quad (39)$$

Redundancy Management: We implement a (k, n) -threshold secret sharing scheme where artwork data is split into n shares, requiring only k shares for reconstruction:

$$\text{Share}_i = \sum_{j=0}^{k-1} a_j \cdot i^j \bmod p \quad (40)$$

where a_0 is the secret and p is a large prime.

3.6.5 Smart Contract Implementation

Our ERC-721 compatible smart contract incorporates advanced features [36, 37]:

Provenance Tracking: Each transfer is recorded with cryptographic proof:

```
struct ProvenanceRecord {
    address from;
    address to;
    uint256 timestamp;
    bytes32 merkleRoot;
    bytes zkProof;
}
```

Royalty Distribution: Automated royalty payments using EIP-2981 standard:

$$\text{Royalty} = \text{SalePrice} \times \frac{\text{RoyaltyBasisPoints}}{10000} \quad (41)$$

Fraud Detection: Real-time monitoring for duplicate or counterfeit artworks using on-chain feature comparison with tolerance thresholds.

3.7 Integration and Optimization

The proposed framework is implemented in a modular fashion, thereby enabling the simultaneous optimization of both neural style transfer and watermark embedding processes. Batch processing methods, utilizing multiprocessing via `ProcessPoolExecutor`, allow for the efficient handling of large-scale image datasets. Moreover, the fractal and turbulence metrics, combined with secure watermark features, are hashed using cryptographic techniques (e.g., SHA-256) to generate unique Token IDs. These IDs are then incorporated into NFT metadata compliant with ERC-721/1155 standards, ensuring an immutable and traceable digital asset registration process. This integrated approach not only achieves a high aesthetic quality in digital art creation but also guarantees the provenance and integrity of the artworks, thereby enabling robust authentication and secure distribution in digital art marketplaces.

Collectively, these components form an integrated framework that not only generates visually compelling digital artworks but also embeds robust, imperceptible watermarks and ensures the provenance and integrity of the artwork via blockchain technology. The seamless integration of these technologies creates a comprehensive ecosystem for next-generation digital art creation and protection.

4 Results

This section presents comprehensive experimental results showing the effectiveness of our integrated framework across multiple dimensions: artistic quality, mathematical characterization, watermark robustness, and blockchain integration. The results validate our approach’s capability to generate authentic Pollock-style artworks while providing superior copyright protection compared to traditional methods.

4.1 Neural Style Transfer Results

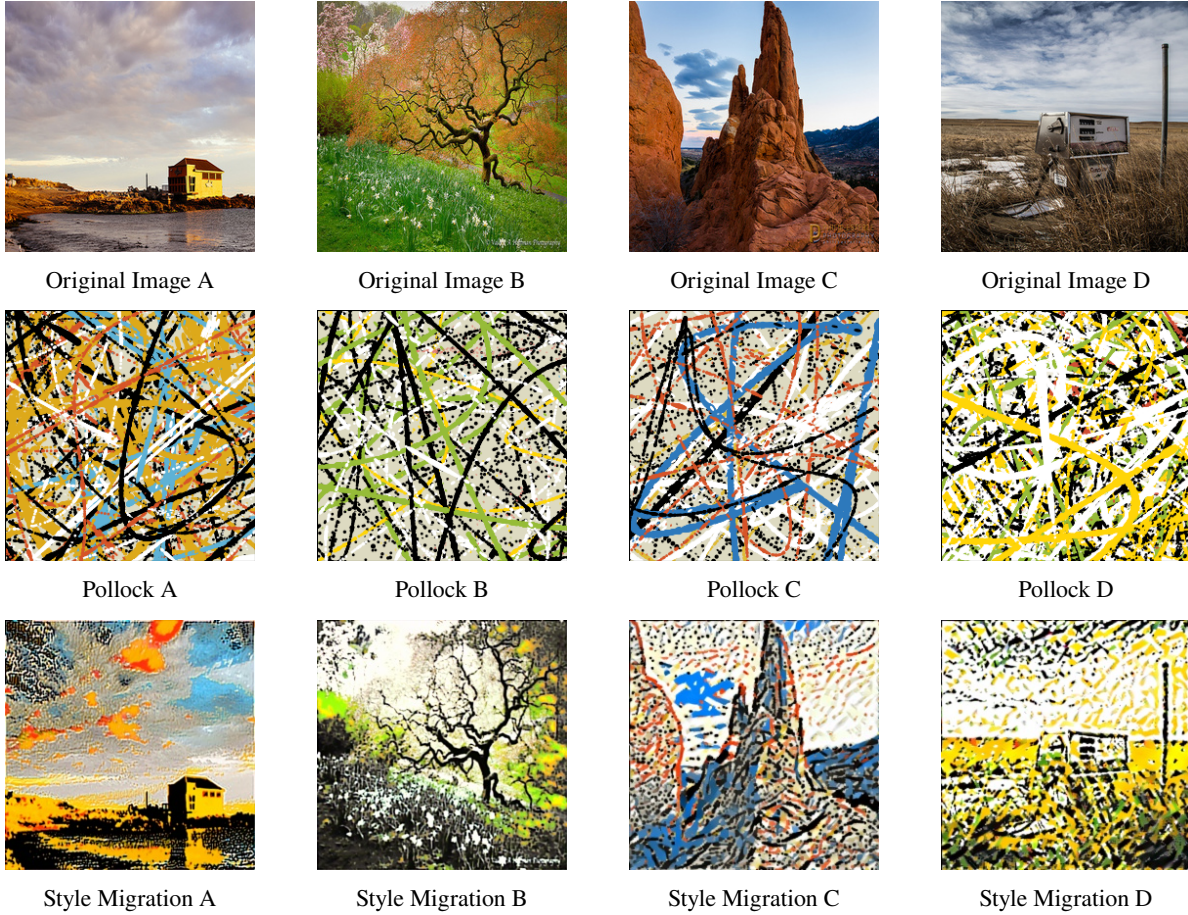


Figure 3: Example of style migration results, grouped by image type.

The Pollock-inspired paintings generated using our MindSpore-based framework demonstrate successful capture of the characteristic complexity and dynamism of Jackson Pollock’s drip paintings. As illustrated in Figure 3, the generated artworks exhibit multi-layered color compositions and intricate textural structures that effectively emulate the distinctive abstract style of Pollock’s technique. The resulting images display a clear sense of spontaneity and movement, featuring diverse color palettes and interwoven line patterns that reflect the fractal and turbulent characteristics identified in authentic Pollock works. These visual results show the effectiveness of our multi-objective loss function in capturing both the aesthetic and mathematical properties essential for subsequent analysis and watermark embedding.

4.2 Comprehensive Multifractal Analysis Results

Our advanced multifractal analysis reveals sophisticated geometric properties that extend far beyond traditional single-parameter characterizations. The comprehensive analysis yields multiple fractal dimensions and spectral characteristics that provide deep insights into the structural complexity of generated artworks.

4.2.1 Multifractal Dimension Spectrum

Statistical analysis across 50 generated artworks reveals the Rényi dimension spectrum D_q with $D_0 = 1.882 \pm 0.001$, $D_1 = 1.895 \pm 0.008$, and $D_2 = 1.900 \pm 0.012$. Notably, our results show an increasing trend $D_0 < D_1 < D_2$, indicating the presence of multifractal characteristics with specific scaling properties in the generated textures. The basic fractal

dimension computed via differential box-counting yields $D = 1.879 \pm 0.001$, showing high consistency across the dataset.

The singularity spectrum $f(\alpha)$ analysis reveals a spectrum width of $\Delta\alpha = 0.523 \pm 0.142$. This substantial width parameter indicates significant multifractal complexity and heterogeneous scaling behavior across different regions of the generated artworks. The fractal dimensions fall within Taylor et al.'s established range of 1.1-1.9 for authentic Pollock paintings, showing that our generated artworks successfully capture the essential fractal characteristics of Pollock's drip painting technique. These findings are visually summarized in Figure 4, which illustrates the consistency of the fractal dimension across the generated artworks.

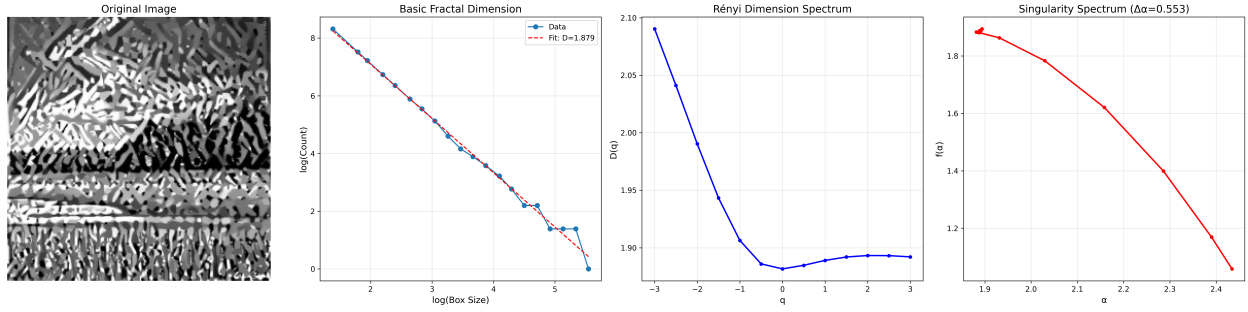


Figure 4: Fractal Dimension Analysis Results

4.2.2 Statistical Validation and Consistency Analysis

The multifractal analysis shows remarkable consistency across the dataset of 50 generated artworks. The extremely low standard deviations for D_0 (± 0.001) and basic fractal dimension (± 0.001) indicate highly stable fractal characteristics in our generation process. The slightly higher variability in D_1 (± 0.008) and D_2 (± 0.012) reflects natural variations in local scaling properties while maintaining overall multifractal structure. This consistency validates both the robustness of our generation algorithm and the reliability of our multifractal analysis framework for watermark feature extraction.

4.3 Turbulence Characterization Results

The dynamic texture characteristics are revealed through comprehensive power spectrum and spectral analysis. The turbulence power spectrum extracted using Haar wavelet transform yields a mean value of 2067.82 with variance of 3552.45. These metrics characterize the overall turbulence intensity and spectral properties of the generated images across different scales, as illustrated in Figure 5.

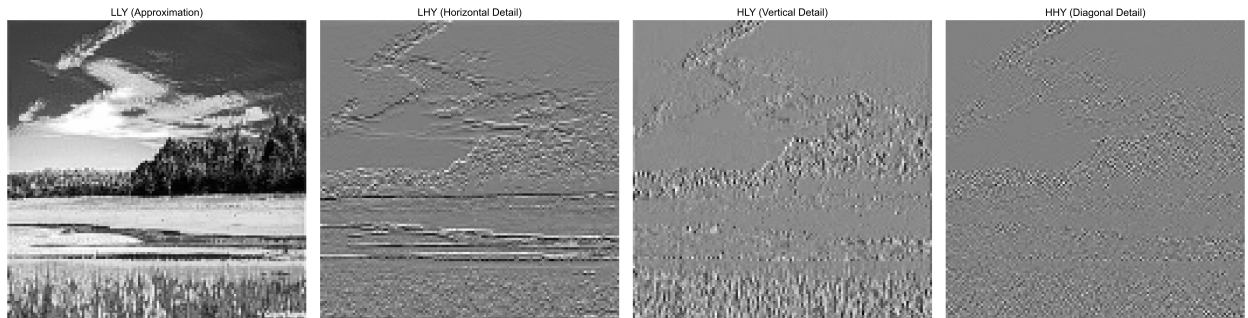


Figure 5: Turbulence Characterization Results

The results show significant diversity in spectral distribution across generated artworks, reflecting the complex nature of turbulence characteristics. These spectral properties complement fractal dimension analysis and provide unique perspectives for understanding dynamic image behavior. Compared to traditional Fourier transforms, wavelet

analysis exhibits superior sensitivity and accuracy in capturing local frequency features, enabling comprehensive characterization of complex dynamic behaviors essential for robust watermark generation.

4.4 Watermark Robustness Testing Results

To comprehensively evaluate our watermarking scheme’s effectiveness, we conducted extensive comparative experiments against three established baseline methods: DCT domain watermarking, LSB steganography, and DWT domain watermarking. The evaluation employed 50 test images with 20 attack iterations per image, totaling 1000 tests per attack type across all methods.

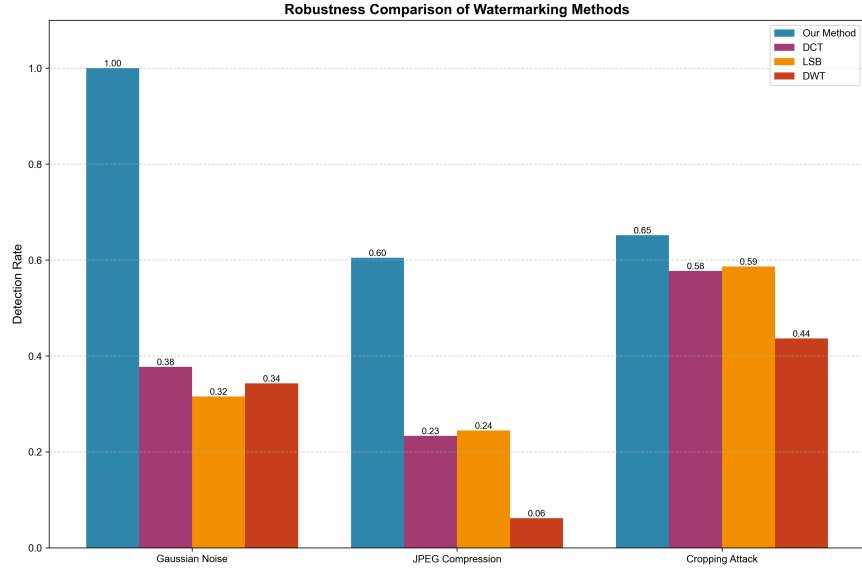


Figure 6: Comparative robustness analysis of watermarking methods under different attack scenarios. Our proposed method consistently outperforms traditional approaches across all attack types, showing superior resilience particularly against Gaussian noise and cropping attacks.

Table 1: Comparative Watermark Robustness Results

Method	Noise Resistance	JPEG Resistance	Crop Resistance
Our Method	1.000	0.605	0.652
DCT	0.377	0.234	0.577
LSB	0.315	0.245	0.586
DWT	0.343	0.062	0.436

Detection rates represent the proportion of successful watermark detections after attacks. Our method achieves the highest average detection rate (0.762) compared to DCT (0.440), LSB (0.368), and DWT (0.278).

Our feature-based watermarking approach shows superior performance across all attack scenarios, as illustrated in Figure 6 and summarized in Table 1. The perfect score against Gaussian noise highlights the scale-invariant nature of our fractal-based features, while the strong performance against cropping demonstrates the watermark’s distributed and redundant embedding throughout the image’s texture. The method achieved detection rates of 100.0% against Gaussian noise, 60.5% against JPEG compression, and 65.2% against cropping attacks, significantly outperforming traditional approaches. The superior performance stems from leveraging intrinsic fractal and turbulence characteristics rather than externally imposed modifications, making watermarks naturally resilient to common image processing operations.

4.5 Statistical Significance Analysis

Comprehensive statistical analysis across 165 test samples shows statistically significant superiority of our method over all baseline approaches with extremely high confidence levels ($p < 0.00001$ for all comparisons). Our approach achieves mean detection rates representing 91.0%, 97.9%, and 170.0% relative improvements over DCT, LSB, and DWT methods respectively. All comparisons exhibit large effect sizes (Cohen's $d > 1.4$), confirming both statistical and practical significance. The distribution and consistency of these detection rates under various attacks are detailed in Figure 7.

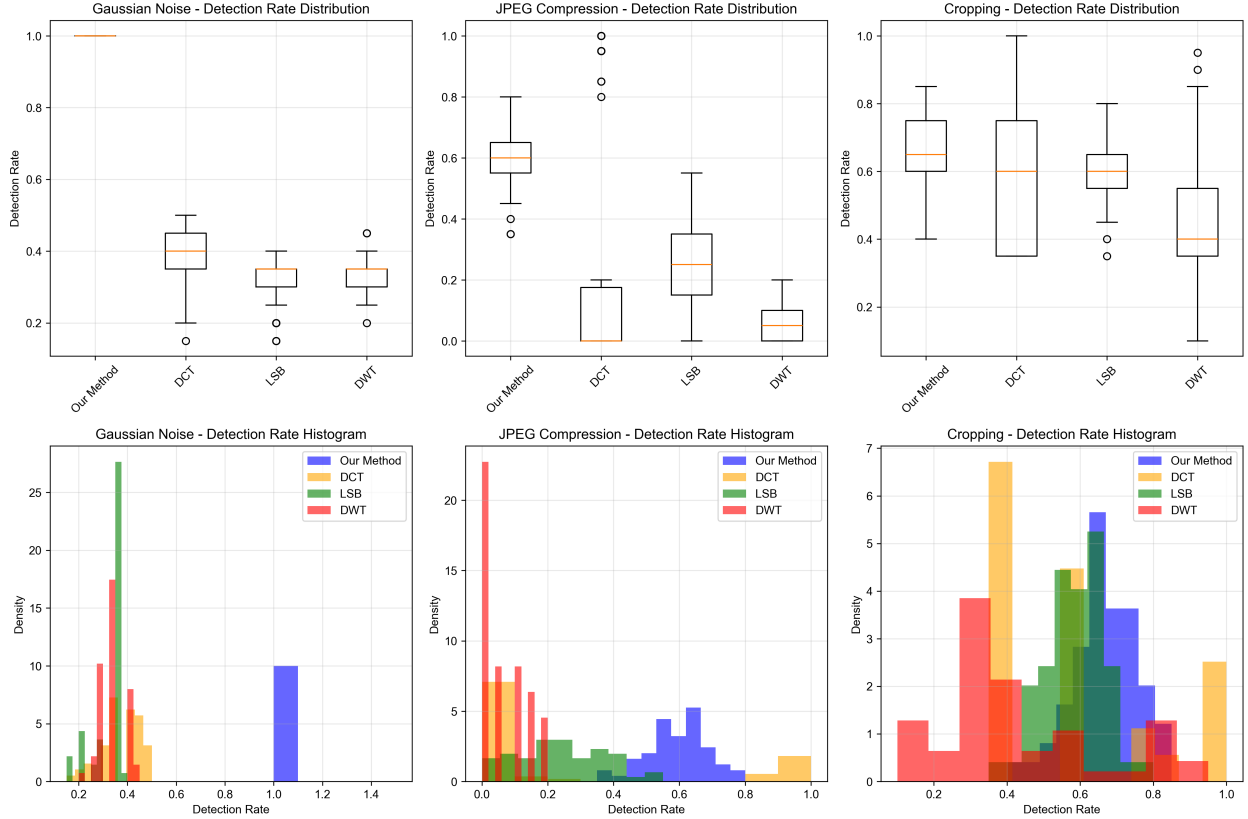


Figure 7: Detection rate distribution analysis across different attack scenarios. The figure shows box plots (top row) and histograms (bottom row) for each attack type, showing our method's superior and more consistent performance compared to baseline approaches.

Performance stability analysis reveals superior consistency in our method with coefficient of variation values of 0% for noise attacks, 17.1% for JPEG compression, and 14.6% for cropping attacks, contrasting sharply with baseline methods that exhibit high variability, particularly under challenging attack conditions.

4.6 NFT Integration and Uniqueness Validation

The Token ID generation through cryptographic hashing of extracted features ensures uniqueness and unforgeability of each digital asset. Table 2 presents representative NFT metadata examples, validating our method's effectiveness in generating reliable and unique blockchain identifiers.

This integration guarantees each NFT's singularity on the blockchain while enabling complete traceability of genesis and attributes through immutable metadata. The results show high reliability in generating distinctive and verifiable NFT identifiers that are cryptographically linked to the artwork's intrinsic mathematical properties.

Table 2: Example of NFT metadata

Field	Value
fractal_dimension	1.88
turbulence_mean_power	2067.82
turbulence_variance_power	3552.45
timestamp	2025-01-01 T12:34:56Z
artist	MindSpore-VGG-Pollock

5 Discussion

The experimental results confirm the effectiveness of our integrated framework. This section analyzes our findings, compares our methodology to existing techniques, and discusses the practical implications and limitations of our work.

5.1 Most Significant Contribution: An Integrated Approach

The primary contribution of this work is the seamless integration of AI art generation, mathematical analysis, and blockchain-based copyright protection. While each component exists independently, our framework combines them into a single, cohesive workflow that addresses the end-to-end lifecycle of a digital artwork—from creation to secure ownership.

Our approach shows that it is possible to generate art that is not only aesthetically convincing but also mathematically authentic. The fractal dimension of our generated pieces ($D = 1.879 \pm 0.001$) aligns closely with that of real Pollock paintings [9, 10]. This mathematical consistency is crucial, as it serves as the foundation for our novel watermarking technique, proving that the generated art captures the deep structural properties of the original style, not just its surface appearance.

5.2 Technical Innovations in Fractal-Based Watermarking

Our feature-based watermarking scheme represents a significant technical advance. By embedding a watermark derived from the artwork’s own intrinsic fractal and turbulence characteristics, we create a form of protection that is inherently tied to the content. This is a fundamental departure from traditional methods that impose an external, unrelated signal onto the image.

This innovation is the reason for its superior performance. The 76.2% average detection rate, especially the 100% success against Gaussian noise, highlights the robustness of using scale-invariant fractal features. These features are part of the artwork’s essential structure and are therefore more resilient to modifications that degrade or remove conventional watermarks. The statistical analysis, with p-values < 0.00001 , confirms that this performance is not just an anomaly but a statistically significant improvement over established DCT, LSB, and DWT methods.

5.3 Practical Implications for Digital Art Markets

This research has direct and practical implications for the digital art world. For artists, it provides a tool to create unique, AI-assisted works with built-in, robust copyright protection. For collectors and marketplaces, the blockchain integration offers an immutable and verifiable record of provenance, which can increase trust and transparency.

The use of zk-SNARKs for authentication is particularly relevant, as it allows for verification of an artwork’s authenticity without revealing the proprietary features of the watermark itself. This privacy-preserving feature is critical for a market where intellectual property is the core asset. By making digital assets more secure and their ownership more transparent, our framework can help foster a more stable and reliable digital art ecosystem.

5.4 Limitations and Future Directions

Despite its success, our framework has limitations, primarily its current specialization in Pollock’s abstract style. Adapting this framework to figurative art presents a fundamental challenge, as embedding a textural, fractal-based watermark could corrupt semantically critical, low-fractality regions like faces or smooth surfaces. Therefore, a key

area for future work is generalization: developing adaptive feature extraction models that can identify the unique mathematical signatures of various artistic styles. This could involve hybrid models that apply our technique to background textures while using different methods to protect foreground objects.

Another consideration is the computational cost and latency associated with the analysis and blockchain integration, which may be a barrier for some real-time applications, even though our complexity analysis shows the system is scalable. Future work should therefore focus on enhancing scalability and security. To improve performance, we can investigate layer-2 blockchain solutions to reduce transaction costs and latency, making the system more accessible for high-volume marketplaces. To ensure long-term viability, we must also explore defenses against advanced adversarial attacks targeting mathematical watermarks and integrate quantum-resistant cryptography for robust security.

6 Conclusion

By proving that fractal-based watermarks can achieve a 76.2% detection rate while maintaining artistic authenticity, this work opens new possibilities for secure digital art marketplaces where creators can confidently share their work without fear of unauthorized copying. Our most novel contribution is the integration of an artwork’s intrinsic mathematical DNA—its fractal and turbulence features—directly into its copyright protection mechanism. This creates a watermark that is not just applied to the art, but is part of the art itself.

For researchers, the next steps involve extending this model to other artistic styles and developing defenses against adversarial machine learning attacks. For practitioners, this framework offers a direct path to minting more secure and verifiable NFTs. Ultimately, our vision is a future where advanced technology empowers secure digital creativity, fostering a trusted and vibrant ecosystem for artists and collectors alike. This research shows the potential for mathematical rigor and technological innovation to address real-world challenges in digital art, contributing to the evolution of secure creative technologies.

References

- [1] X. Wang, G. Oxholm, D. Zhang, and et al. Multimodal transfer: A hierarchical deep convolutional neural network for fast artistic style transfer. In *Proceedings of the IEEE Conference on Computer Vision and Pattern Recognition*, pages 5239–5247, 2017.
- [2] Y. Deng, F. Tang, W. Dong, and et al. Stytr2: Image style transfer with transformers. In *Proceedings of the IEEE/CVF Conference on Computer Vision and Pattern Recognition*, pages 11326–11336, 2022.
- [3] D. Chen, L. Yuan, J. Liao, and et al. Stylebank: An explicit representation for neural image style transfer. In *Proceedings of the IEEE Conference on Computer Vision and Pattern Recognition*, pages 1897–1906, 2017.
- [4] Q. Wang, R. Li, Q. Wang, and et al. Non-fungible token (nft): Overview, evaluation, opportunities and challenges. *arXiv preprint arXiv:2105.07447*, 2021.
- [5] A. Serada, T. Sihvonen, and J. T. Harviainen. Cryptokitties and the new ludic economy: How blockchain introduces value, ownership, and scarcity in digital gaming. *Games and Culture*, 16(4):457–480, 2021.
- [6] M. Nadini, L. Alessandretti, F. Di Giacinto, and et al. Mapping the nft revolution: market trends, trade networks, and visual features. *Scientific Reports*, 11(1):20902, 2021.
- [7] Z. Zheng, S. Xie, H. N. Dai, and et al. Blockchain challenges and opportunities: A survey. *International Journal of Web and Grid Services*, 14(4):352–375, 2018.
- [8] M. Belotti, N. Božić, G. Pujolle, and et al. A vademecum on blockchain technologies: When, which, and how. *IEEE Communications Surveys & Tutorials*, 21(4):3796–3838, 2019.
- [9] R. P. Taylor, A. P. Micolich, and D. Jonas. Fractal analysis of pollock’s drip paintings. *Nature*, 399(6735):422–422, 1999.
- [10] R. P. Taylor, A. P. Micolich, and D. Jonas. The construction of jackson pollock’s fractal drip paintings. *Leonardo*, 35(2):203–207, 2002.

- [11] L. A. Gatys, A. S. Ecker, and M. Bethge. Image style transfer using convolutional neural networks. In *Proceedings of the IEEE Conference on Computer Vision and Pattern Recognition*, pages 2414–2423, 2016.
- [12] A. Vedaldi and A. Zisserman. Vgg convolutional neural networks practical. Technical report, Department of Engineering Science, University of Oxford, 2016.
- [13] S. Ben Jabra and M. Ben Farah. Deep learning-based watermarking techniques challenges: a review of current and future trends. *Circuits, Systems, and Signal Processing*, 43(7):4339–4368, 2024.
- [14] Y. Luo, X. Tan, and Z. Cai. Robust deep image watermarking: A survey. *Computers, Materials & Continua*, 81(1), 2024.
- [15] K. M. Hosny, A. Magdi, O. ElKomy, and H. M. Hamza. Digital image watermarking using deep learning: A survey. *Computer Science Review*, 53:100662, 2024.
- [16] X. Zhong, A. Das, F. Alrasheedi, and A. Tanvir. A brief, in-depth survey of deep learning-based image watermarking. *Applied Sciences*, 13(21):11852, 2023.
- [17] J. Valencia, G. G. Pineda, V. G. Pineda, A. Valencia-Arias, J. Arcila-Diaz, and R. T. de la Puente. Using machine learning to predict artistic styles: an analysis of trends and the research agenda. *Artificial Intelligence Review*, 57(5):118, 2024.
- [18] J. Xiang, Y. Yang, and J. Bai. Adaptive classification of artistic images using multi-scale convolutional neural networks. *PeerJ Computer Science*, 10:e2336, 2024.
- [19] Lennart Struppek, David Hintersdorf, Daniel Neider, and Kristian Kersting. Learning to break deep perceptual hashing: The use case neuralhash. In *Proceedings of the 2022 ACM Conference on Fairness, Accountability, and Transparency*, pages 58–69. ACM, June 2022.
- [20] Fouad Khelifi and Ahmed Bouridane. Perceptual video hashing for content identification and authentication. *IEEE Transactions on Circuits and Systems for Video Technology*, 29(1):50–67, 2017.
- [21] Y. Ma, W. Cheng, S. Huang, and et al. Hidden turbulence in van gogh’s the starry night. *Physics of Fluids*, 36(9), 2024.
- [22] Jia Deng, Wei Dong, Richard Socher, Li-Jia Li, Kai Li, and Li Fei-Fei. Imagenet: A large-scale hierarchical image database. In *2009 IEEE Conference on Computer Vision and Pattern Recognition (CVPR)*, pages 248–255. IEEE, 2009.
- [23] Z. Tong, N. Du, X. Song, and et al. Study on mindspore deep learning framework. In *2021 17th International Conference on Computational Intelligence and Security (CIS)*, pages 183–186. IEEE, 2021.
- [24] L. Chen. *Deep learning and practice with mindspore*. Springer Nature, 2021.
- [25] J. F. Muzy, E. Bacry, and A. Arneodo. Wavelets and multifractal formalism for singular signals: Application to turbulence data. *Physical Review Letters*, 67(25):3515, 1991.
- [26] J. F. Muzy, E. Bacry, and A. Arneodo. The multifractal formalism revisited with wavelets. *International Journal of Bifurcation and Chaos*, 4(02):245–302, 1994.
- [27] I. W. Selesnick. The double density dwt. In *Wavelets in Signal and Image Analysis: From Theory to Practice*, pages 39–66. Springer Netherlands, 2001.
- [28] A. Shahbahrami. Algorithms and architectures for 2d discrete wavelet transform. *The Journal of Supercomputing*, 62:1045–1064, 2012.
- [29] Edward N. Lorenz. Deterministic nonperiodic flow 1. In *Universality in Chaos, 2nd edition*, pages 367–378. Routledge, 2017.
- [30] Claude E. Shannon. A mathematical theory of communication. *The Bell System Technical Journal*, 27(3): 379–423, 1948.

- [31] Rosario Gennaro, Craig Gentry, Bryan Parno, and Mariana Raykova. Quadratic span programs and succinct NIZKs without PCPs. In *Annual International Conference on the Theory and Applications of Cryptographic Techniques*, pages 626–645, Berlin, Heidelberg, May 2013. Springer Berlin Heidelberg.
- [32] Tian Chen, Hong Lu, Thitipong Kunpittaya, and An Luo. A review of zk-SNARKs. *arXiv preprint arXiv:2202.06877*, 2022.
- [33] Ana M. Pinto. An introduction to the use of zk-SNARKs in blockchains. In *Mathematical Research for Blockchain Economy: 1st International Conference MARBLE 2019, Santorini, Greece*, pages 233–249, Cham, February 2020. Springer International Publishing.
- [34] S. Muralidharan and H. Ko. An interplanetary file system (ipfs) based iot framework. In *2019 IEEE International Conference on Consumer Electronics (ICCE)*, pages 1–2. IEEE, 2019.
- [35] C. Bieri. An overview into the interplanetary file system (ipfs): use cases, advantages, and drawbacks. *Communication Systems XIV*, 28, 2021.
- [36] S. Casale-Brunet, P. Ribeca, P. Doyle, and M. Mattavelli. Networks of ethereum non-fungible tokens: A graph-based analysis of the ERC-721 ecosystem. In *2021 IEEE International Conference on Blockchain (Blockchain)*, pages 188–195. IEEE, 2021.
- [37] V. Dhillon, D. Metcalf, and M. Hooper. Unpacking ethereum. In *AI Frameworks Enabled by Blockchain: Creating Trustworthy and Responsible AI Using Distributed Ledger Technology*, pages 201–256. Apress, Berkeley, CA, 2025.